Electronic structure of MnO

A. Fujimori
Department of Physics, University of Tokyo, Bunkyo-ku, Tokyo 113, Japan

N. Kimizuka, T. Akahane, T. Chiba, and S. Kimura
National Institute for Research in Inorganic Materials, Tsukuba, Ibaraki 305, Japan

F. Minami
Research Institute of Applied Electricity, Hokkaido University, Sapporo 060, Japan

K. Siratori
Department of Physics, Osaka University, Toyonaka 560, Japan

M. Taniguchi
Department of Materials Science, Hiroshima University, Hiroshima 730, Japan

S. Ogawa
Synchrotron Radiation Laboratory, Institute for Solid State Physics, University of Tokyo, Tanashi, Tokyo 188, Japan

S. Suga
Department of Material Physics, Osaka University, Toyonaka 560, Japan
(Received 29 March 1990)

We have studied the electronic structure of MnO by photoemission spectroscopy. Mn $3d$-derived emission is found to be confined within ~ 10 eV of the top of the valence band, and we find no evidence for an intrinsic satellite at higher binding energies. The photoemission intensity of the whole valence band is enhanced for photon energies in the Mn $3p \rightarrow 3d$ core absorption region. These observations suggest that d^4 and $d^5\underline{L}$ photoemission final states ($\underline{L}$ denotes a ligand hole) are close in energy and are strongly hybridized with each other. The spectra are analyzed in terms of configuration-interaction theory using a MnO_6 cluster model. We thus find that the ligand-to-Mn d charge-transfer energy Δ is comparable to the intra-atomic Coulomb energy $U \simeq 7.5$ eV. Namely, MnO is indeed close to the boundary between the Mott-Hubbard ($U < \Delta$) and the charge-transfer ($U > \Delta$) regimes in the Zaanen-Sawatzky-Allen phase diagram, and the d^4 and $d^5\underline{L}$ states are nearly degenerate. The large Δ value leads to a highly ionic character in the Mn—O bonding.

I. INTRODUCTION

Recently, there has been increasing interest in the electronic structure of $3d$ transition-metal oxides stimulated by new information obtained by photoemission spectroscopy[1] and by the discovery of high-T_c superconductivity in doped Cu oxides.[2] It seems now widely accepted that insulting oxides of late $3d$ transition metals such as CuO and NiO are not Mott-Hubbard insulators in the original sense but are charge-transfer insulators.[3,4] That is, the band gaps of these materials are formed between the O $2p$ band and the $3d$ upper Hubbard band separated by the ligand-to-metal charge-transfer energy Δ, an energy required for $d^n \rightarrow d^{n+1}\underline{L}$.[5,6] Oxides of early $3d$ elements (Ti, V) are classified in the Mott-Hubbard regime, where band gaps of magnitude $\sim U$ are formed between the upper and lower Hubbard bands because $\Delta > U$. So far, photoemission studies have revealed that FeO is in the charge-transfer regime[7] while VO is certainly in the Mott-Hubbard regime.[8] Therefore MnO or (hypothetical) CrO should be located near the boundary between the two regimes since Δ and U are expected to vary systematically as a function of the atomic number of the transition metal.

In this work, we have studied MnO by photoemission spectroscopy with subsequent analyses using a configuration-interaction cluster model. The electronic configuration of the Mn^{2+} (d^5) ion in MnO is rather simple in its ground state: The spin-up part of the Mn $3d$ shell is fully occupied, leading to a ^6S (or $^6A_{1g}$ under the cubic symmetry) state. MnO had long been regarded as a typical Mott-Hubbard insulator, but was recently proposed to be a change-transfer insulator[9] in analogy to NiO. The present results indicate that MnO is intermediate between the Mott-Hubbard and charge-transfer insulators or is marginally a charge-transfer insulator.

II. EXPERIMENTAL PROCEDURE

X-ray photoemission-spectroscopy (XPS) and ultraviolet photoemission-spectroscopy (UPS) measurements

were carried out in a spectrometer equipped with a Mg x-ray source ($h\nu=1253.6$ eV), a He resonance lamp ($h\nu=21.2$ and 40.8 eV), and a double-pass cylindrical-mirror analyzer. UPS measurements were also done at beamline 2 of the Synchrotron Radiation Laboratory, where photons were monochromatized by a modified Rowland-mount monochromator. Samples were introduced into the spectrometers having a base pressure of $\sim 1\times 10^{-10}$ Torr and were scraped *in situ* with a diamond file to obtain clean surfaces. All measurements were done at room temperature because experiments at liquid-nitrogen temperature were unsuccessful due to charging of the samples. The energy resolution of the XPS, He UPS, and synchrotron-radiation UPS measurements were about 1, 0.2, and 0.5 eV, respectively.

We have studied an undoped (pure) MnO single crystal and a MnO polycrystal doped with FeO_x. The pure sample is a single crystal grown by the floating-zone method in a high-pressure (20 kg/cm^2) Ar atmosphere. Its O-to-Mn ratio could be accurately determined to be 1.003 by measuring the weight increase when oxidized to Mn_3O_4.[10] As this sample is highly insulating, some photoemission measurements were unsuccessful due to charging effect. Therefore, we prepared an electrically conductive sample by mixing conductive, isostructural FeO_x (wustite, $x\sim 0.9$) into MnO. This sample is a polycrystalline pellet made by sintering a mixture of 88.9 mol % MnO (99.9% purity) and 11.1 mol % Fe_2O_3 (99.99% purity) powders at 1200 °C for ~ 2 h in a 2:1 mixture of CO_2 and H_2. It was confirmed by x-ray diffraction to be an 8:2 solid solution of MnO and FeO_x having the NaCl-type structure.[11] The lattice constant of the doped sample was smaller than that of MnO only by 0.017 Å, which should have negligible effects on the electronic structure studied here. As we shall see below, Mn $3d$-derived photoemission features are largely determined by the Mn $3d$ intra-atomic and the nearest-neighbor Mn-O interactions. The spectra of the FeO_x-doped sample are consistent with 8:2 superpositions of the MnO and FeO_x spectra, without indication of interaction between the Fe and Mn $3d$ states.

III. RESULTS

Figure 1 shows valence-band XPS and UPS spectra of both samples. Synchotron-radiation UPS measurements on the pure sample were unsuccessful due to a strong broadening of the spectra due to a charging of the sample, whereas measurements using the He lamp merely resulted in a small energy shift and a weak broadening. (The reason for the absence of strong charging effect for the He UPS is not known.) XPS spectra of the same sample showed a uniform shift of ~ 10 eV toward higher binding energies. Therefore the spectra of the pure sample shown in Fig. 1 have been aligned to those of the FeO_x-doped sample which showed no charging.

Figure 1 shows that the spectra of both samples are virtually identical except for weak features at higher binding energies $E_B\simeq 10$–12 eV and a slight broadening for the pure sample due to charging. Lad *et al.*[9] have observed for cleaved MnO single crystals a weak emission peak exactly at the same position as in the present doped

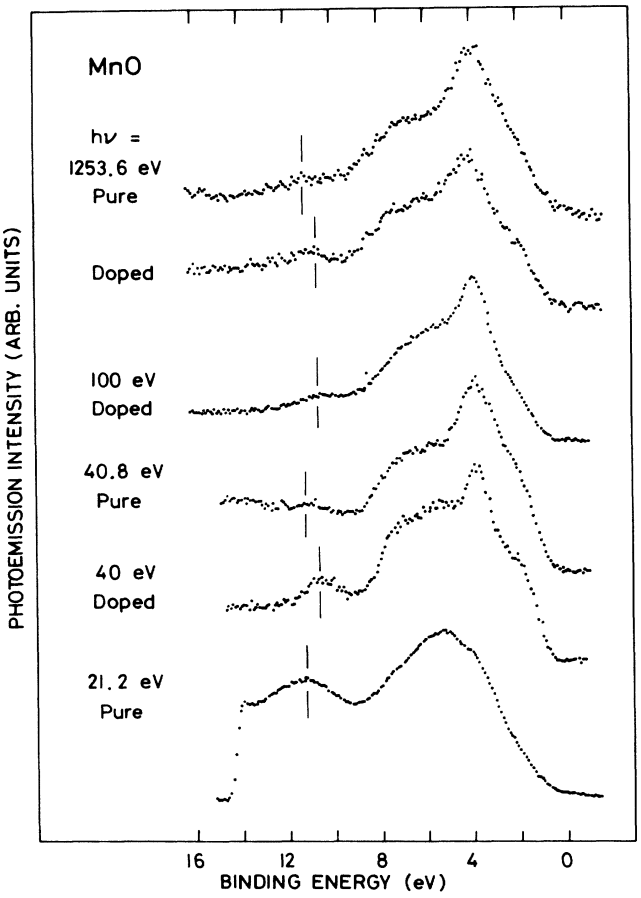

FIG. 1. Valence-band XPS and UPS spectra of the pure MnO single crystal and the FeO_x-doped MnO polycrystal. The vertical bars mark a feature at $E_B\simeq 11$ eV for the pure sample and a contamination-related feature at $E_B\simeq 10.5$ eV for the doped sample.

sample, i.e., at $E_B\simeq 10.5$ eV, which they assigned to a satellite of the intrinsic bulk origin. Eastman and Freeouf[12] have also observed a similar peak at the same position for a cleaved MnO single crystal (see Fig. 2). However, this emission does not seem to be an intrinsic bulk feature of MnO but would rather arise from contamination such as impurity or grain boundary phases, oxygen defects, adsorbed oxygen, hydroxide, etc., since in our experiment it is considerably weaker and is shifted by ~ 0.5 eV toward higher binding energies for the pure single crystal. Note that the single crystals studied by Lad *et al.* contained ~ 7 at. % of α-Mn_3O_4 for an impurity phase.[9] The 10.5-eV feature becomes more intense for lower photon energies, consistent with its primarily O $2p$ origin. On the other hand, the fact that this feature remains observable for XPS and that it exhibits appreciable enhancement in the Mn $3p\rightarrow 3d$ core absorption region (see below) indicates that there is also a significant mixture of Mn $3d$ character into this feature. Presumably this feature is related to impurity-phase Mn oxides other than MnO.

Figure 3 shows UPS spectra of the doped sample taken at photon energies in the Mn $3p\rightarrow 3d$ absorption region. Photoemission from the Mn $3d^5$ configuration is

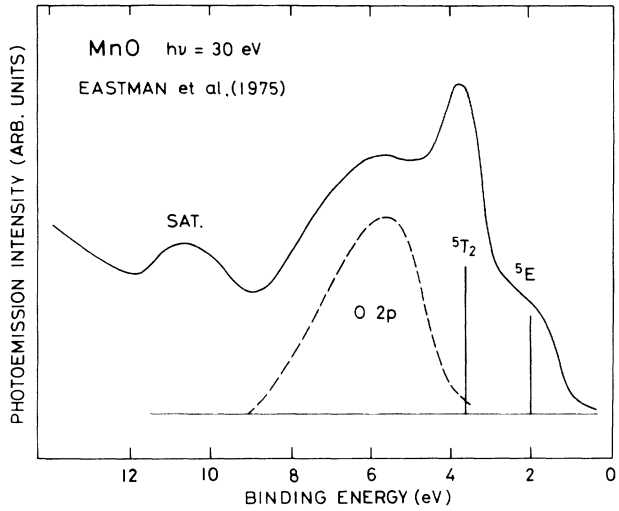

FIG. 2. Valence-band UPS spectrum of MnO and its assignment based on ligand-field theory (Ref. 12). The heights of vertical bars are proportional to the theoretical photoemission intensities. (In Ref. 12, the relative intensities have been incorrectly given as $^5E_g:^5T_{2g}=1:1$.) The binding energy scale has been shifted so as to approximately coincide with ours.

enhanced through interference between the direct emission, $3d^5+h\nu\rightarrow 3d^4+\epsilon l$, and the core excitation followed by a super Coster-Kronig decay, $3p^63d^5+h\nu\rightarrow 3p^53d^6\rightarrow 3p^63d^4+\epsilon l$.[1,3] The intensity of the whole valence band reaches a maximum at $h\nu\simeq 50$ eV and a minimum at $h\nu\simeq 48$ eV. The dominant peak at $E_B\simeq 4$ eV and the shoulder at $E_B\simeq 2$ eV exhibit the most remarkable enhancement for $h\nu\simeq 50$ eV and are almost completely suppressed for $h\nu\simeq 48$ eV [and are largely suppressed for our lowest photon energy $h\nu=21.2$ eV (Fig. 1)], indicating that these features are due to Mn $3d$-electron emission. The bottom panel of Fig. 3 shows the difference curve between the spectra for $h\nu=50.5$ and 48 eV, representing the Mn $3d$-derived photoemission. (The intensities have been normalized to the photon flux prior to subtraction.) The difference curve shows that the structures at $E_B\simeq 6$ and 10.5 eV have some Mn $3d$ admixture through they are mainly derived from O $2p$.

The resonance behavior of the photoemission spectra is more clearly seen in the constant-initial-state (CIS) spectra shown in Fig. 4, where photoemission intensities at various binding energies are plotted as functions of photon energy. There one can see a tendency that the resonance peak in the CIS spectra is more pronounced for higher-binding-energy features and the antiresonance dip for lower-binding-energy features. This tendency, however, is much less pronounced (except for $E_B=10.2$ eV, which is probably extrinsic) than in the case of charge-transfer insulators, NiO,[13,14] FeO_x,[7] and Fe_2O_3.[15] The resonance behavior of MnO is rather uniform for the whole valence-band region. This indicates that no clear separation of the spectra into $d^5\underline{L}$ and d^4 final states is possible for MnO, unlike the charge-transfer insulators, implying that the d^4 and $d^5\underline{L}$ final states are overlapping and/or strongly hybridizing with each other.

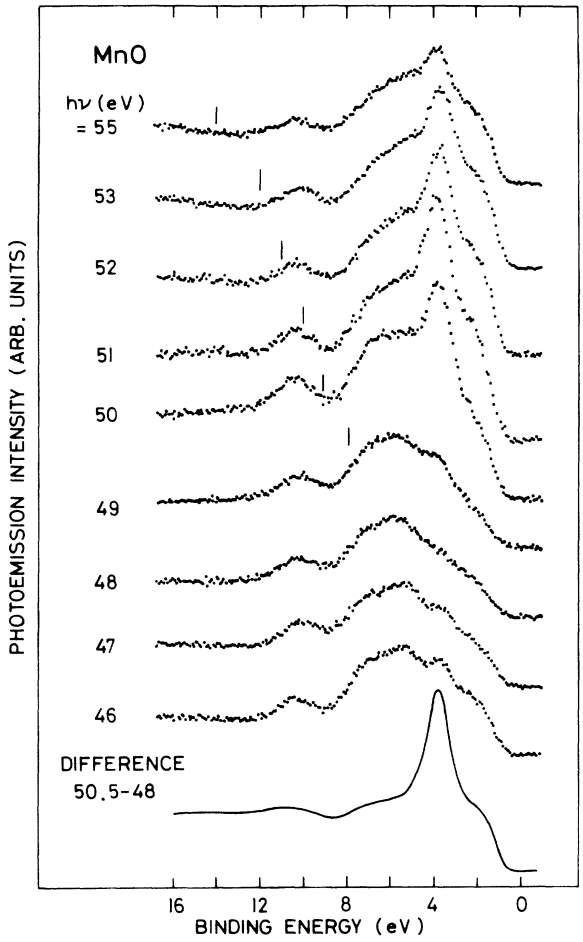

FIG. 3. Valence-band UPS spectra of the FeO_x-doped MnO polycrystal for photon energies in the Mn $3p\rightarrow 3d$ core absorption region. The vertical bars mark the kinetic energy of the Mn $M_{2,3}M_{4,5}M_{4,5}$ Auger peak. The bottom panel shows the difference between the on-resonance ($h\nu=50.5$ eV) and off-resonance ($h\nu=48$ eV) spectra normalized to the photon flux, and represents the Mn $3d$-derived photoemission.

One also notices in Fig. 4 that some CIS spectra ($E_B=3.7$, 7.1, and 10.2 eV) show a weak peak at $h\nu\simeq 47$ eV while others ($E_B=1.7$ and 5.3 eV) do not. This peak corresponds to the ^6D final state of the $3p\rightarrow 3d$ absorption of the Mn^{2+} ion whereas the dominant peak at $h\nu\sim 50$ eV corresponds to the ^6P final state.[16] This observation might be used to identify the symmetry of the photoemission final states if the corresponding super-Coster-Kronig transition-matrix elements were known, but in the present study such an attempt has not been made.

The CIS spectra and the total-yield curve in Fig. 4 show structures at $h\nu\simeq 54$–57 eV, which coincides with the Fe $3p\rightarrow 3d$ absorption features of FeO_x.[7] As these CIS features are weak and separated from the Mn $3p\rightarrow 3d$ absorption, they can be ignored for the study of the Mn $3d$ resonance behaviors. The valence-band photoemission spectra of FeO_x show a broad main band centered at $E_B\sim 4$ eV as well as a broad satellite centered at $E_B\sim 12$ eV,[7] which may explain the subtle difference between the photoemission spectra of the pure and FeO_x-doped samples (Fig. 1).

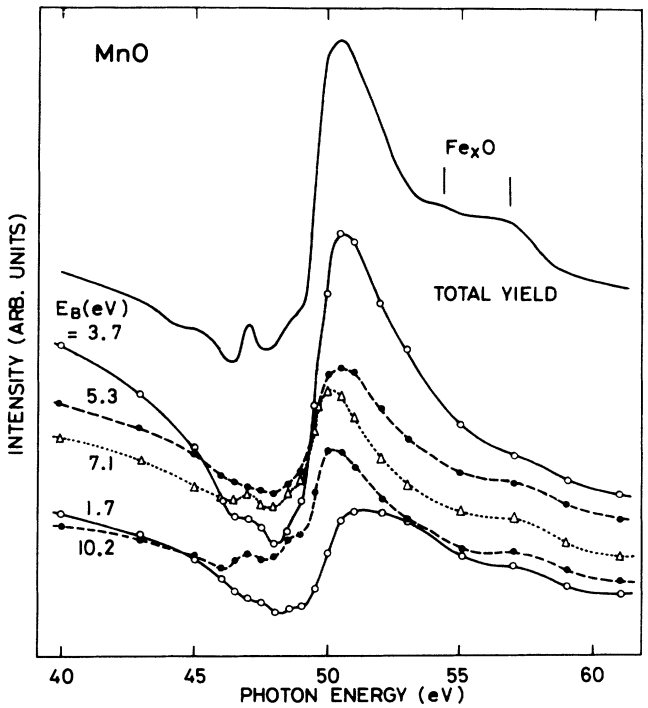

FIG. 4. CIS and total-yield spectra of the FeO_x-doped MnO polycrystal in the Mn $3p \rightarrow 3d$ core absorption region.

IV. ANALYSES AND DISCUSSION

A. Ligand-field theory

The interpretation of the photoemission spectra of MnO and other insulating Mn^{2+} compounds has traditionally been based on ligand-field theory, i.e., on the $d^5 \rightarrow d^4$ multiplet structure in a cubic ligand field.[12,17] The only allowed d^4 multiplet state is ^5D, which is split into $^5T_{2g}$ and ^5E_g states by the ligand field. This type of spectral assignment is shown in Fig. 2,[12] where the structures at $E_B \approx 2$, 4, and 6 eV are attributed to the ^5E_g, $^5T_{2g}$, and the O $2p$ band, respectively. This localized atomic picture, however, does not predict the resonance enhancement of the 6-eV band in the Mn $3p \rightarrow 3d$ absorption region. Further the ligand-field theory predicts a Mn $3d$ feature at $E_B \sim 2$ eV, which is too strong or too sharp compared with the experimental result as seen in Fig. 2. In order to overcome these difficulties, we have to explicitly take into account hybridization between the Mn $3d$ and O $2p$ states and/or that between neighboring Mn $3d$ ions. Such departures from the atomic localized picture will be considered below.

B. One-electron band theory

An opposite approach to the electronic structure of MnO is one-electron band theory, in which each electron is assumed to occupy an itinerant Bloch state. Spin-polarized band-structure calculations with the actual antiferromagnetic ordering (AF II structure) yield fully occupied majority-spin Mn $3d$ bands which are split into t_{2g} and e_g bands.[18,19] These two bands may correspond to the photoemission signals at $E_B \simeq 4$ and 2 eV, respectively. The Mn $3d$ contribution to the O $2p$ band at ~ 6 eV may be interpreted as due to one-electron Mn $3d$–O $2p$ hybridization,[9,18] although the calculated amount of Mn d character hybridized into the O $2p$ band[18] appears too weak to explain the experimental result. According to the calculations, the e_g band is broadened considerably on going from the antiferromagnetic to the paramagnetic states, which may explain the broadness of the 2-eV emission since the experiments have been done above the Néel temperature $T_N = 122$ K.[19] An experimental test for this would be to see whether the 2-eV feature becomes sharper below T_N. Unfortunately, we could not measure spectra at low temperatures because of the charging problem even for the FeO_x-doped sample.

Thus unlike in the case of $Cd_{1-x}Mn_xTe$, where an additional Mn $3d$–derived feature (satellite) is observed well below the Te $5p$–derived valence band and disagreement with band theory is quite obvious,[20,21] there have been no serious, qualitative discrepancies between band theory and experiment in the case of MnO, at least for the line shape of the Mn d–derived photoemission spectra. We will see below, however, that the reasonable agreement is rather fortuitous and that the one-electron picture is not appropriate to describe the electronic structure of MnO.

It is interesting to note that there is a good correspondence between the assignment made by ligand-field theory and that made by band theory. In both cases, the photoemission features at $E_B \simeq 2$ and 4 eV are ascribed to emission of Mn $3d$ electrons having e_g- and t_{2g}-symmetry Mn $3d$ electrons, respectively. The integrated intensities of these features should therefore be 2:3. This is because of the closed-shell structure of the high-spin ground state of the Mn^{2+} ion, for which the multiplet structures of the allowed $d^5 \rightarrow d^4$ and $d^5 \rightarrow d^6$ transitions are identical to the occupied and unoccupied one-electron Mn d energy levels, respectively.

C. Configuration-interaction theory

As in the previous analyses of the photoemission spectra of other high-spin d^5 systems, Fe_2O_3, and $Cd_{1-x}Mn_xTe$,[15,20] we have applied a configuration-interaction theory to an octahedral $(MnO_6)^{10-}$ cluster consisting of the central Mn^{2+} ion and surrounding O^{2-} atoms. The ground state of the cluster is given as a hybridized state between the purely ionic configuration, $Mn^{2+}(O^{2-})_6$, and O $2p \rightarrow$ Mn $3d$ charge-transferred states representing the Mn $3d$–O $2p$ covalent contribution:[14]

$$\Psi_g(^6A_{1g}) = a|d^5\,^6A_{1g}\rangle + b|d^6\underline{L}\,^6A_{1g}\rangle \ . \quad (1)$$

Here, only states with $^6A_{1g}$ symmetry are retained. Summation over $\underline{L}_\sigma$ and $\underline{L}_\pi$ is implicitly assumed in the second term on the right-hand side of Eq. (1). The final states of d-electron photoemission are given in the form

$$\Psi_f(^{2S+1}\Gamma) = a_f|d^4\,^{2S+1}\Gamma\rangle + b_f|d^5\underline{L}\,^{2S+1}\Gamma\rangle \ , \quad (2)$$

where $^{2S+1}\Gamma$ denotes the symmetry of the final state. The first term in Eq. (2) represents a d-hole state (d^4

state) produced by direct d-electron emission from the d^5 component of the ground state (1) and the second term ligand-hole states produced by charge-transfer screening of the d-hole state as well as by direct d-electron emission from the $d^6\underline{L}$ component of the ground state. A limited number of $d^6\underline{L}^2$ states have also been included in Eq. (2).[15]

Using the above model, we have reproduced the valence-band XPS spectrum of the pure MnO sample. The mean energies of the d^5, $d^6\underline{L}$, d^4, $d^5\underline{L}$, and $d^6\underline{L}^2$ configurations and the transfer integral $(pd\sigma)$ between Mn $3d$ and O $2p$ are treated as adjustable parameters. [We have assumed $(pd\pi)=-0.5(pd\sigma)$ according to Harrison.[22]] As for Racah parameters B and C, the free-ion values[23] of Mn^{2+} and Mn^{3+} are used for the d^5 and d^4 configurations and extrapolated values for the d^6 configuration. The calculated spectrum has been convoluted with Gaussian and Lorentzian functions in order to simulate the instrumental, lifetime, and other broadening effects. Large parts of the O $2p$ states that do not hybridize with Mn $3d$ states are represented by overlapping two Gaussians centered at $E_B \simeq 4.5$ and 6 eV. The Gaussians reproduce the O $2p$ band of MgO,[24] which has the same crystal structure as MnO but has no d electrons. The intensity of the O $2p$ band relative to the Mn $3d$-derived emission is taken to be three times larger than the theoretical photoionization cross sections[25] as a usual practice.[3,15] For the details of the calculation, the reader is referred to Refs. 3 and 15.

The best fit of the calculated spectrum to the measured XPS is obtained as shown in Fig. 5 with the following parameter values: $\Delta \equiv E(d^6\underline{L})-E(d^5)=7\pm1$ eV, $U \simeq [E(d^6\underline{L})-E(d^5)]-[E(d^5\underline{L})-E(d^4)]=7.5\pm0.05$ eV, and $(pd\sigma)=-2(pd\pi)=-0.9\pm0.05$ eV. One can see from Fig. 5 that the calculation reproduces all the characteristic features of the XPS spectrum with correct binding energies and intensities, i.e., the dominant peak at $E_B \simeq 4$ eV, the shoulder at $E_B \approx 2$ eV, and the Mn d contribution around $E_B \sim 6$ eV. It is noted that both ^5E_g and $^5T_{2g}$ characters are present in each of the 2- and 4-eV features. These features are not pure ^5E_g and $^5T_{2g}$ states, as predicted by the ligand-field theory or band theory.

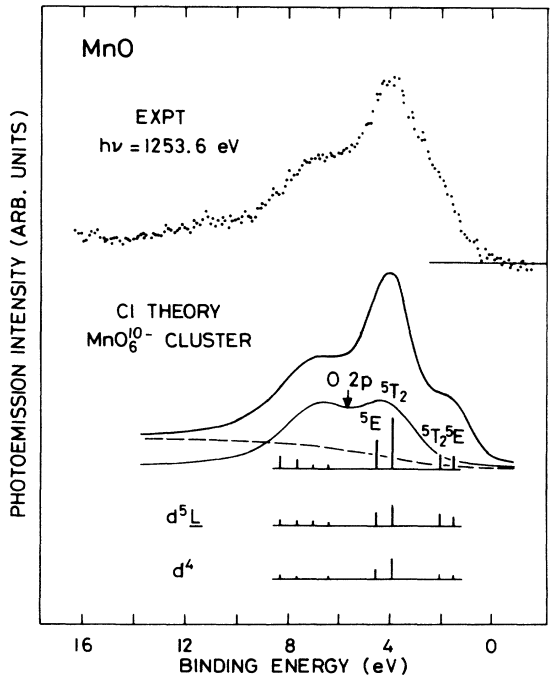

FIG. 5. Theoretical XPS spectrum calculated using configuration-interaction theory on the $(MnO_6)^{10-}$ cluster model compared with the experimental XPS spectrum of the pure MnO single crystal. The calculated spectrum is decomposed into d^4 and $d^5\underline{L}$ final-state components.

The fitted parameter values reveals that $\Delta \sim U$ (or Δ is slightly smaller than U), which indicates that MnO is located close to the boundary between the Mott-Hubbard and charge-transfer regimes in the Zaanen-Sawatzky-Allen phase diagram.[5] That is, states close to the top of the valence band as well as states well below them are due to strong mixtures of Mn $3d$-hole and O $2p$-hole states (d^4 and $d^5\underline{L}$), since $E(d^4)-E(d^5\underline{L}) \simeq \Delta - U \sim 0$. This is clearly seen in the decomposition of the final states into d^4 and $d^5\underline{L}$ components as shown in Fig. 5. The strong d^4-$d^5\underline{L}$ hybridization is also consistent with the Mn $3p \rightarrow 3d$ resonance behavior that the whole valence band shows relatively uniform resonance enhancement.

Because of the large Δ value, ~ 7 eV, the Mn $3d$-O $2p$ covalency in the ground state is expected to be rather weak. Namely, we find the ground state (1) to contain only 6% $d^6\underline{L}$ configuration, whereas using the same analysis NiO is shown to have $\sim 10\%$ $d^9\underline{L}$ configuration,[3] Fe_2O_3 to have $\sim 20\%$ $d^6\underline{L}$ (Ref. 15), and high-T_c Cu oxides to have $\sim 35\%$ $d^{10}\underline{L}$ (Ref. 26). The increase of Δ on going from Cu to Ni to Mn monoxides, which is an expected chemical tendency, leads to the weak Mn $3d$-O $2p$ covalency. (The covalency of Fe_2O_3 is unusually strong because the Fe is trivalent.) This situation is schematically depicted in Fig. 6, where MnO and NiO are compared. Our fitted Δ value for MnO is ~ 3 eV larger than that for NiO. This difference between NiO and MnO agrees with that estimated by Zaanen and Sawatzky using the atomic ionization energies and Madelung potentials.[27]

The transfer integral $(pd\sigma) \simeq -0.9$ eV estimated for MnO is 77% of NiO (-1.17 eV) (Ref. 3) and 60% of Fe_2O_3 (-1.5 eV).[15] These ratios are somewhat smaller than those predicted by the relation $(pd\sigma) \sim r_d^{1.5}/d^{3.5}$, where r_d is a characteristic radius of the $3d$ element (listed in the "Solid State Table of the Elements" of Ref. 22) and d is the interatomic distance.[22] Namely, the $(pd\sigma)$ of MnO is predicted to be about the same as that of NiO and $\sim 80\%$ of Fe_2O_3. Tight-binding fits to the energy-band structures by Mattheiss[28] has given the MnO to NiO ratio for $(pd\sigma)$ to be 95%. The absolute $(pd\sigma)$ value for MnO is $\sim 90\%$ of Mattheiss's value.[28]

The additional photoemission feature located at $E_B \simeq 10.5$ eV, which has previously been assigned to a d^4 satellite in analogy to NiO,[9] cannot be reproduced in the present cluster calculation. This may give further support to our opinion that this feature is not an intrinsic one. As for the peak at $E_B \simeq 11$ eV of the pure single-crystal sample, we cannot completely rule out the possibility that it is an intrinsic feature related, e.g., to $d^6\underline{L}^2$ or

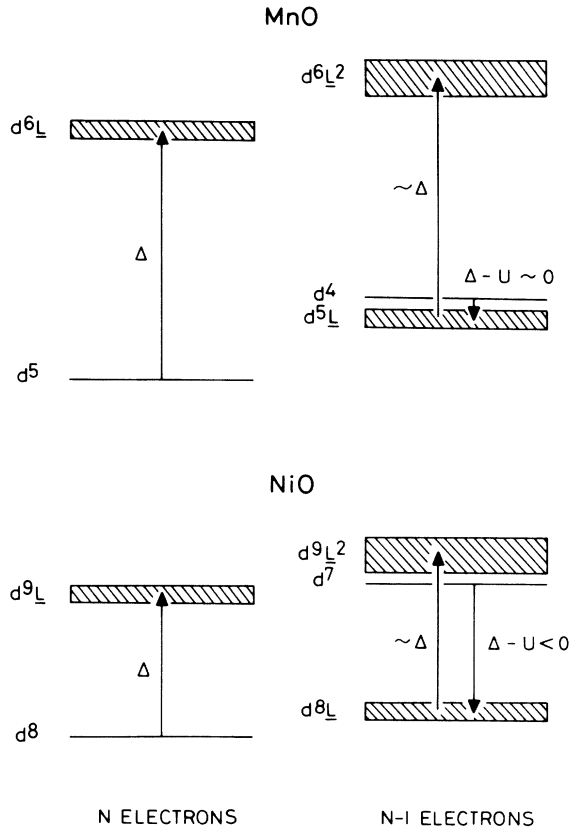

FIG. 6. Schematic energy-level diagrams for the ground states (N-electron system) and the photoemission final states ($N-1$-electron system) of MnO and NiO. The multiplet splittings and the p-d hybridization effects are not shown. The actual $\underline{L}$ bandwidths are wider than shown.

higher-order states which have not been fully taken into account in our cluster calculation, although its growth for $h\nu=21.2$ eV strongly suggests an extrinsic origin.

As for the unoccupied electronic states of MnO, the expected Mn $3d$-derived inverse-photoemission or bremsstrahlung isochromat spectroscopy (BIS) spectra are relatively simple. The only allowed component, ^5D, of the $d^5 \rightarrow d^6$ multiplet will be the dominant Mn d-derived feature, and its splitting into ^5E_g and $^5T_{2g}$ would be extremely small. A much weaker $d^7\underline{L}$ feature will be located at higher energies separated by $\sim\Delta+U$. The energy position of the ^5D state can be estimated following the procedure of Ref. 15. We estimate the ^5D state to be ~ 8 eV above the top of the valence band, which may be further lowered by 1–2 eV by a d^6 band formation and/or by extra relaxations not considered in the model. The interband absorption starts at $h\nu\simeq 4.5$ eV in the optical spectra,[29] which is ~ 2 eV smaller than estimated above. This discrepancy may be due to the limited accuracy of the cluster model in predicting the energies of the unoccupied states from the information about the occupied states, or may be due to optical transitions of a different origin (e.g., transition into Mn $4s$ states) occurring at lower energies than the O $2p$-to-Mn $3d^6$ transition. Future BIS experiments will resolve this problem.

V. CONCLUSION

We have studied the electronic structure of MnO by photoemission spectroscopy and a configuration-interaction cluster-model analysis. The experimental and theoretical results indicate that d^4 and $d^5\underline{L}$ final states are nearly degenerate and are strongly hybridized with each other. Namely, the O $2p$-to-Mn $3d$ charge-transfer energy Δ is comparable to the Mn $3d$ intra-atomic Coulomb energy U, locating MnO in the boundary region between the Mott-Hubbard and the charge-transfer regimes of the Zaanen-Sawatzky-Allen phase diagram. The Mn $3d$-O $2p$ transfer integrals are by ~ 20 and $\sim 40\%$ smaller than those of NiO and Fe_2O_3, respectively. These variations in the electronic-structure parameters of MnO, NiO, and Fe_2O_3 shown are consistent with chemical trends and roughly with other theoretical estimates. The charge-transfer energy Δ of MnO is large, leading to a highly ionic character in the Mn—O bonding.

ACKNOWLEDGMENTS

We would like to thank K. Soda, T. Mori, and the staff of the Synchrotron Radiation Laboratory for valuable technical support.

[1]For review see, e.g., L. C. Davis, J. Appl. Phys. **59**, R25 (1986).
[2]See, e.g., K. C. Hass, in *Solid State Physics*, Vol. 41, edited by H. Ehrenreich and D. Turnbull (Academic, Boston, 1989), p. 213.
[3]A. Fujimori, F. Minami, and S. Sugano, Phys. Rev. B **29**, 5225 (1984); A. Fujimori and F. Minami, *ibid.* **30**, 957 (1984).
[4]J. Ghijsen, L. H. Tjien, J. van Elp, H. Eskes, J. Weternik, G. A. Sawatzky, and M. T. Czyzyk, Phys. Rev. B **38**, 11 322 (1988).
[5]J. Zaanen, G. A. Sawatzky, and J. W. Allen, Phys. Rev. Lett. **55**, 418 (1985).
[6]S. Hüfner, Z. Phys. B **61**, 135 (1985).
[7]A. Fujimori, N. Kimizuka, M. Taniguchi, and S. Suga, Phys. Rev. B **36**, 6691 (1987).
[8]S. Shin, S. Suga, M. Taniguchi, M. Fujisawa, H. Kanzaki, A. Fujimori, H. Daimon, Y. Ueda, K. Kosuge, and S. Kachi, Phys. Rev. B **41**, 4993 (1990).
[9]R. J. Lad and V. E. Henrich, Phys. Rev. B **38**, 10 860 (1988).
[10]W. C. Hahn and A. Muan, Am. J. Sci. **258**, 66 (1960).
[11]R. W. Gurry and L. S. Darken, J. Am. Chem. Soc. **72**, 3909 (1950).
[12]D. E. Eastman and J. L. Freeouf, Phys. Rev. Lett. **34**, 395 (1975).
[13]M. R. Thuler, R. L. Benbow, and Z. Hurych, Phys. Rev. B **27**, 2028 (1983).
[14]S.-J. Oh, J. W. Allen, I. Lindau, and J. C. Mikkelsen, Phys. Rev. B **26**, 4845 (1982).
[15]A. Fujimori, M. Saeki, N. Kimizuka, M. Taniguchi, and S. Suga, Phys. Rev. B **34**, 7318 (1986).
[16]R. Bruhn, E. Schmidt, H. Schröder, and B. Sonntag, Phys.

Lett. **90A**, 41 (1982).
[17]T. Ishii, S. Kono, S. Suzuki, I. Nagakura, T. Sagawa, R. Kato, M. Watanabe, and S. Sato, Phys. Rev. B **12**, 4320 (1975).
[18]K. Terakura, T. Oguchi, A. R. Williams, and J. Kubler, Phys. Rev. B **30**, 4734 (1984).
[19]E. J. Ojala and K. Terakura, Phys. Rev. B **33**, 2733 (1986).
[20]L. Ley, M. Taniguchi, J. Ghijsen, R. L. Johnson, and A. Fujimori, Phys. Rev. B **35**, 2839 (1987); M. Taniguchi, A. Fujimori, M. Fujisawa, T. Mori, I. Souma, and Y. Oka, Solid State Commun. **62**, 431 (1987).
[21]A. Franciosi, A. Wall, Y. Gao, J. H. Weaver, M. -H. Tsai, J. Dow, R. V. Kasowski, R. Reifenberger, and F. Pool, Phys. Rev. B **40**, 12 009 (1989).
[22]W. A. Harrison, *Electronic Structure and the Physical Properties of Solids* (Freeman, San Francisco, 1980).
[23]Y. Tanabe and S. Sugano, J. Phys. Soc. Jpn. **9**, 767 (1954).
[24]S. P. Kowalczyk, F. R. McFeely, L. Ley, V. T. Gritsyna, and D. A. Shirley, Solid State Commun. **23**, 161 (1977).
[25]J. H. Scofield, J. Electron Spectrosc. Relat. Phenom. **8**, 129 (1976).
[26]A. Fujimori, Phys. Rev. B **39**, 793 (1989).
[27]J. Zaanen and G. A. Sawatzky, Can. J. Phys. **65**, 1262 (1987).
[28]L. F. Mattheiss, Phys. Rev. B **5**, 290 (1972).
[29]L. Messick, W. C. Walker, and R. Glosser, Phys. Rev. B **6**, 3941 (1972).